ResearchGate

See discussions, stats, and author profiles for this publication at: https://www.researchgate.net/publication/227590043

Highly Ordered Mesoporous Silicon Carbide Ceramics With Large Surface Areas and High Stability

ARTICLE *in* ADVANCED FUNCTIONAL MATERIALS · JANUARY 2006

Impact Factor: 11.81 · DOI: 10.1002/adfm.200500643

CITATIONS
113

READS
65

8 AUTHORS, INCLUDING:

Yan Meng
Chinese Academy of Sciences
29 PUBLICATIONS **3,979** CITATIONS
SEE PROFILE

Dehong Chen
University of Melbourne
52 PUBLICATIONS **2,275** CITATIONS
SEE PROFILE

Available from: Dehong Chen
Retrieved on: 26 January 2016

ADVANCED FUNCTIONAL MATERIALS

FULL PAPER

DOI: 10.1002/adfm.200500643

Highly Ordered Mesoporous Silicon Carbide Ceramics with Large Surface Areas and High Stability**

By *Yifeng Shi*, *Yan Meng*, *Dehong Chen*, *Shujiang Cheng*, *Peng Chen*, *Haifeng Yang*, *Ying Wan*, and *Dongyuan Zhao**

Highly ordered mesoporous silicon carbide ceramics have been successfully synthesized with yields higher than 75 % via a one-step nanocasting process using commercial polycarbosilane (PCS) as a precursor and mesoporous silica as hard templates. Mesoporous SiC nanowires in two-dimensional (2D) hexagonal arrays (*p6m*) can be easily replicated from a mesoporous silica SBA-15 template. Small-angle X-ray diffraction (XRD) patterns and transmission electron microscopy (TEM) images show that the SiC nanowires have long-range regularity over large areas because of the interwire pillar connections. A three-dimensional (3D) bicontinuous cubic mesoporous SiC structure (*Ia3d*) can be fabricated using mesoporous silica KIT-6 as the mother template. The structure shows higher thermal stability than the 2D hexagonal mesoporous SiC, mostly because of the 3D network connections. The major constituent of the products is SiC, with 12 % excess carbon and 14 % oxygen measured by elemental analysis. The obtained mesoporous SiC ceramics are amorphous below 1200 °C and are mainly composed of randomly oriented β-SiC crystallites after treatment at 1400 °C. N_2-sorption isotherms reveal that these ordered mesoporous SiC ceramics have high Brunauer–Emmett–Teller (BET) specific surface areas (up to 720 $m^2 g^{-1}$), large pore volumes (~0.8 $cm^3 g^{-1}$), and narrow pore-size distributions (mean values of 2.0–3.7 nm), even upon calcination at temperatures as high as 1400 °C. The rough surface and high order of the nanowire arrays result from the strong interconnections of the SiC products and are the main reasons for such high surface areas. XRD, N_2-sorption, and TEM measurements show that the mesoporous SiC ceramics have ultrahigh stability even after re-treatment at 1400 °C under a N_2 atmosphere. Compared with 2D hexagonal SiC nanowire arrays, 3D cubic mesoporous SiC shows superior thermal stability, as well as higher surface areas (590 $m^2 g^{-1}$) and larger pore volumes (~0.71 $cm^3 g^{-1}$).

1. Introduction

Non-oxide ceramics, such as silicon carbides, silicon nitrides, and boron nitrides, have been investigated intensively in various research areas because of their unique mechanical and functional characteristics.[1–5] Silicon carbides with high thermal conductivity, high thermal stability, excellent mechanical strength, and chemical inertness are especially considered as effective catalyst supports for many reactions in harsh environments.[6–14] The demand for high surface area and uniform porosity in this application makes the preparation of mesoporous non-oxide ceramics an attractive challenge.[15–20] However, there have been few reports on successfully fabricating ordered mesoporous ceramic structures with high surface areas and large adjustable pores. The difficulties are mainly the extremely high synthesis temperatures, the lack of proper precursors, the necessity of using special non-commercial reagents,[18] and the complexity of the synthetic procedure that requires, e.g., Schlenk techniques and multiple impregnating processes.[21] A sol–gel process,[20] a solid–gas reaction,[22] and a nanocasting process[16] have previously been used to prepare mesoporous SiC ceramics, but the products have been disordered, with a very broad pore-size distribution. Mesostructured SiC/silica composites have been prepared by a chemical-vapor infiltration process using ordered mesoporous silica as a host matrix.[17] After removing the silica matrices, however, the composites showed broad pore-size distributions and no long-range-ordered regularities because of the insufficient SiC loadings.

Preceramic polymers, such as polysilazene, polysilane, polycarbosilanes (PCS), and polymethylsilane, have been widely used to produce ceramics, and particularly non-oxide ceramics, including SiC, Si_3N_4, SiCN, BN, and AlN, because they can be processed at temperatures lower than those required in conventional fabrication methods. Various morphologies such as films, fibers, tubes, and also composites, can be prepared easily from preceramic polymers[16,23–26]. PCS in which a silicon moiety alternates with a carbon moiety in the main chain

[*] Prof. D. Y. Zhao, Y. F. Shi, Y. Meng, D. H. Chen, S. J. Cheng, P. Chen, Dr. H. F. Yang, Dr. Y. Wan
Department of Chemistry
and Molecular Catalysis and Innovative Materials Laboratory
Fudan University, Shanghai 200433 (P.R. China)
E-mail: dyzhao@fudan.edu.cn

[**] This work was supported by NSF of China (20421303, 20233030, 20173012, 20407014), the State Key Basic Research Program of PRC (G200048001, 2002AA321010), and the Shanghai Municipal Scientific Commission (03DJ14004, 03527001, 04JC14087, 03QF14037). We also thank Sumin Zhu from the Shanghai Institute of Ceramics, Chinese Academic of Science, for his helpful advice.

© 2006 WILEY-VCH Verlag GmbH & Co. KGaA, Weinheim

$(SiR_2CH_2)_n$, and which were produced by Yajima as early as 1976, are now recognized as one of the important precursors in the commercial production of SiC fibers. They dissolve well in organic solvents such as tetrahydrofuran (THF) and xylene and are, therefore, favorably disposed to the casting process.[16,25,26]

Here, we demonstrate the successful synthesis of highly ordered mesoporous silicon carbides with unusually high Brunauer–Emmett–Teller (BET) surface areas (430–720 $m^2 g^{-1}$), uniform pore sizes (~3.5 nm), and extremely high thermal stabilities (up to 1400 °C) replicated by mesoporous silica hard templates and commercial PCS precursors via a one-step nanocasting process. Highly ordered two-dimensional (2D) hexagonal (*p6m*) and three-dimensional (3D) bicontinuous gyroidal (*Ia3d*) SiC nanowire arrays have been cast from the hard templates, mesoporous silica SBA-15 and KIT-6, respectively.

2. Results and Discussions

2.1. Replication of the Mesoscale Arrangement

The mesoporous silicas, SBA-15 and KIT-6, were prepared according to the methods reported previously, except that a long aging time (3 days) and high hydrothermal temperature (130 °C) were used.[27,28] This treatment can enhance the mesoporosity of the silica walls[29] and thus enable more connections that stabilize the SiC nanowire arrays. A one-step nanocasting process was employed to prepare PCS–silica hybrid nanocomposites. First, PCS was dissolved in xylene and then mixed well with the hard mesoporous silica templates. Subsequent pyrolysis of PCS and further crystallization were carried out in the mesoporous silica channels under nitrogen using a continuous-heating procedure. Mesoporous silicon carbides were obtained upon fully etching the silica hosts with aqueous HF. The products were labeled as, e.g., SiC-SBA15-1200, to indicate the SBA-15 mesoporous silica host and a final heating temperature of 1200 °C. Compared with a typical two-step casting procedure, this method lacks the second impregnating process.

The symmetry of the silica matrix could be successfully replicated by the mesoporous SiC regardless of the mother template's mesostructure. In addition, increasing the maximum temperature from 1200 to 1400 °C caused no obvious effect on the structural regularity of the mesoporous SiC. Small-angle X-ray diffraction (XRD) patterns of these samples and their mother silica templates are presented in Figure 1 and the cell parameters are listed in Table 1. The data clearly show that the long-range mesoscale periodicities of the host materials have been copied to the mesoporous SiC replicas, although with significant reduction in the cell parameters. The reduction calculated from the *d*-spacing values are about 17 and 22 % for the samples heated at final temperatures of 1200 and 1400 °C, respectively. This phenomenon may be caused by framework shrinkage of the silica hosts, accompanied by a tremendous decrease in the volumes of the pores. This is evidenced by the fact that the mesoporous silica KIT-6 without PCS exhibits a 16 % decrease in cell parameters and a 50 % decrease in pore volume as the calcination temperature is increased from 550 to 900 °C. It is noted that the reduction in the cell-parameter values of the mesoporous SiC is similar to that of the mother silica templates, even though the heating temperature for the former is more than 200 °C higher than that of the latter. This implies that the second step, the impregnating process, which is normally used in the nanocasting of carbon replicas, is unnecessary because the shrinkage of the silica host can compensate for the constriction of the guest agent that arises from the weight loss and densification during the heating.

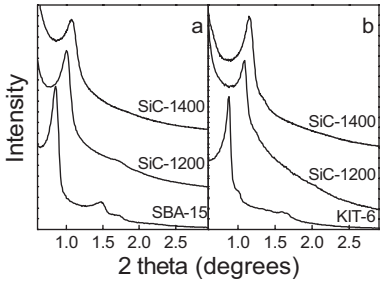

Figure 1. Small-angle XRD patterns of mesoporous silicon carbide replicas and their mother mesoporous silica templates with a) a 2D hexagonal (*p6m*) structure and b) a 3D cubic (*Ia3d*) structure.

Table 1. Textural properties of mesoporous SiC products prepared under different conditions.

No.	Sample name	Cell parameter [nm]	BET surface area [$m^2 g^{-1}$]	Pore size [nm]	Pore volume [$cm^3 g^{-1}$]
a	SiC-SBA15-1200 [a]	9.54	720	2.0	0.52
b	SiC-SBA15-1400 [a]	9.11	580	2.0	0.49
c	SiC-SBA15-1200 [b]	10.2	550	3.6	0.59
d	SiC-SBA15-1400 [b]	9.58	540	3.7	0.58
e	SiC-KIT6-1200 [a]	19.3	460	3.0	0.42
f	SiC-KIT6-1400 [a]	18.8	430	3.5	0.47
g	SiC-KIT6-1200 [b]	20.0	690	3.3, 15	0.79
h	SiC-KIT6-1400 [b]	18.7	620	2.9, 15	0.70

[a] Derived from a silica template treated hydrothermally at 100 °C. [b] Derived from a silica template treated hydrothermally at 130 °C.

Transmission electron microscopy (TEM) investigations also reveal that the structural regularities of the porous structures can be well preserved, as shown in Figure 2. The low-magnification TEM images (Figs. 2a,b) show that the SiC products, which have a uniform size of about 1 μm, have a morphology similar to that of the silica templates. A long-range-ordered mesostructure can be observed in the whole particle domain (Figs. 2a,b). A typical 2D hexagonal mesostructure of the ordered nanowire arrays derived from SBA-15 silica can be observed in the TEM images of SiC-SBA15-1200 (Figs 2c,d). However, the Fourier transformation (Fig. 2d, inset) shows a distorted hexagonal pattern, suggesting that such a high-temperature treatment inevitably causes the mesostructure to distort to some extent. The distance between the centers of the nanowires is about 9 nm, in agreement with the small-angle XRD results (Table 1). TEM images of SiC-KIT6-1400 (Figs. 2e,f) also demonstrate the efficiency of this procedure for

© 2006 WILEY-VCH Verlag GmbH & Co. KGaA, Weinheim

ADVANCED FUNCTIONAL MATERIALS

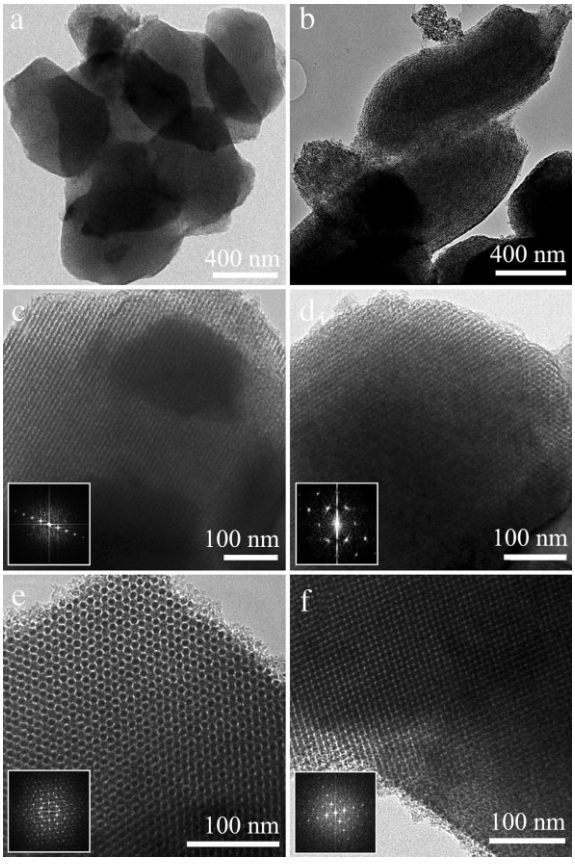

Figure 2. TEM images of mesoporous silicon carbides SiC-SBA15-1200 at low magnification (a,b) and high magnification (c,d) taken along the c) [110] and d) [100] directions. TEM images of SiC-KIT6-1400 taken along the e) [111] and f) [531] directions. Insets show the corresponding Fourier diffractograms.

synthesizing ordered bicontinuous cubic mesoporous SiC ceramics. The cell parameters of the SiC replica determined from TEM measurements and the small-angle XRD pattern are in agreement; the calculated values are 19.4 and 19.8 nm, respectively. They further confirm that the SiC replica that was made using mesoporous silica KIT-6 as the template has a well-ordered bicontinuous cubic *Ia*3*d* mesostructure.

2.2. Chemical Compositions

Figure 3 shows the wide-angle XRD patterns of the mesoporous silica KIT-6, and the mesoporous SiC ceramic derived from KIT-6. No obvious diffraction peaks of SiC crystals can be observed in the XRD patterns when the calcination temperature is lower than 1200 °C, which is indicative of the existence of the amorphous state. The β-SiC phase can be detected in the XRD patterns when the products are heated to above 1200 °C. The diffraction peaks of β-SiC become more intense when the calcination approaches 1400 °C, suggesting that β-SiC is a major constituent of mesoporous SiC. Three diffraction peaks at 2θ values of 35.5, 60.1, and 71.7° are clearly observable, which can be indexed as 111, 200, and 311 planes of β-SiC, according to the standard (Joint Committee on Powder Diffraction Standards (JCPDS) card number 29-1129). This finding suggests that raising the calcination temperature leads to a distinct improvement in the crystallinity. The wide-angle XRD patterns (not shown) of mesoporous SiC ceramics made from SBA-15 mother templates are similar to those of the above-mentioned mesoporous silicon carbides. Some silicon nitrides (Si_3N_4) were formed from the carbothermic reduction of the excess carbon with nitrogen gas and were detected by wide-angle XRD at 1400 °C. Fortunately, the silicon nitrides can be easily removed along with the silica matrix during HF etching. The heating time showed only a minor effect on the crystallinity of the mesoporous SiC walls, since the peak intensities in the XRD patterns remained unaltered upon prolonging the calcination from two to ten hours.

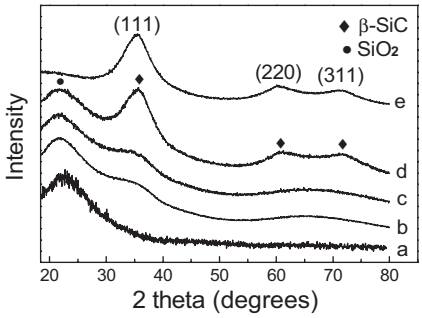

Figure 3. Powder XRD pattern of mesoporous silica KIT-6 (trace a). Powder XRD patterns of SiC/KIT-6 composites heated under N_2 at 1200 °C for 2 h (trace b) and 10 h (trace c); and at 1400 °C for 2 h (trace d); and powder XRD pattern of SiC-KIT6-1400 after the removal of the silica framework (trace e).

The TEM images (Fig. 4) show that the contractions of the ordered SiC nanowires are not uniform (Figs. 4a,c). This finding, together with the absence of clear diffraction fringes of the β-SiC crystal lattice (Fig. 4c), indicate that the obtained nanowires are composed of small-sized β-SiC crystallites. The crystallite size of the SiC-SBA15-1400 sample, evaluated from the wide-angle XRD data using the Scherrer equation, is about 1.5 nm. The selected-area electron diffraction (SAED) pattern of SiC-SBA15-1400 (Fig. 4b) displays three diffraction rings assigned to the 111, 220, and 311 planes, providing further evidence that the mesostructure is composed of β-SiC crystallites with random orientation.

Both the wide-angle XRD patterns (Fig. 3) and the Fourier-transform infrared (FTIR) spectra (Fig. 5) show that the silica matrixes can be removed by HF etching without destroying the ordered mesostructure of the SiC replicas. As shown in Figure 3e, the broad diffraction peak at $2\theta = 22°$, which is attributed to amorphous silica, disappears upon HF etching, while the intense diffraction peaks assigned to β-SiC remain. All the FTIR spectra of the mesoporous SiC replicas display a strong band at around 830 cm^{-1}, which is associated with the Si–C bond, further confirming the existence of silicon carbides after the removal of mesoporous silica. A weak peak at around 1080 cm^{-1} caused by Si–O–Si bonds is also observed, implying that a small amount of oxygen remains after HF etching and may be located on the surface of the SiC nanowires.

© 2006 WILEY-VCH Verlag GmbH & Co. KGaA, Weinheim

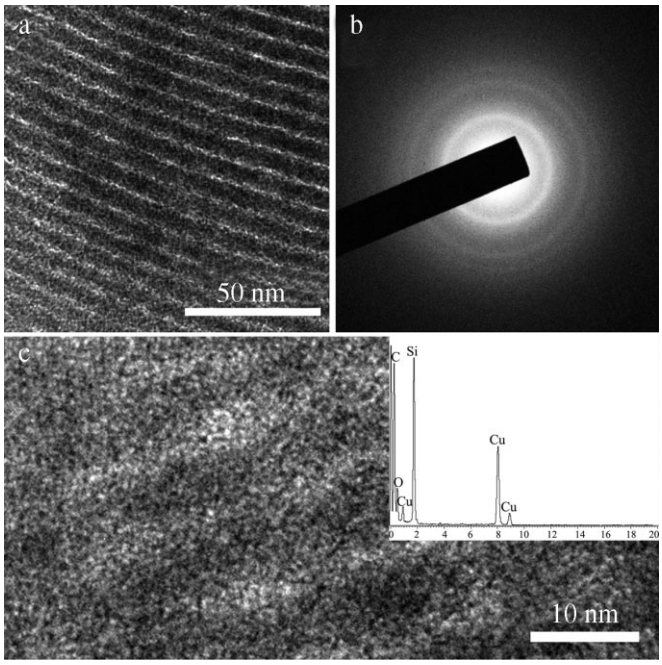

Figure 4. TEM image (a), selected-area electron diffraction (SAED) pattern (b), and high-resolution TEM image (c) of the mesoporous silicon carbide SiC-SBA15-1400. The inset in (c) shows the energy-dispersive X-ray (EDX) spectrum.

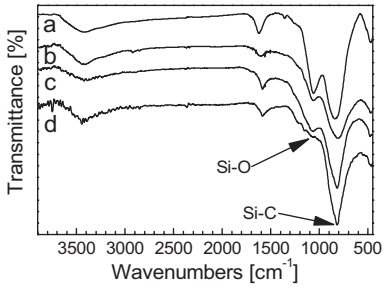

Figure 5. FTIR spectra of mesoporous SiC replicas SiC-SBA15-1200 (trace a), SiC-KIT6-1200 (trace b), SiC-SBA15-1400 (trace c), and SiC-KIT6-1400 (trace d).

Energy-dispersive X-ray spectroscopy (EDX; Fig. 4c, inset) reveals that the SiC product only contains silicon, carbon, and oxygen with compositions of 48, 32, and 14 wt.-%, respectively (determined by elemental analysis). The molar ratio of Si to C is 0.64, which is lower than the stoichiometric ratio of SiC. This is not surprising because, as reported previously, SiC ceramics derived from the pyrolysis of PCS always contain excess carbon and have a low Si/C molar ratio.[23]

The representative thermogravimetric analysis (TGA) curve of the ordered mesoporous SiC measured in air (Fig. 6) indicates that there are three significant weight-change steps. During the first step, which occurs from 25 to 330 °C, a small weight loss of 1.2 % occurs, corresponding to the loss of water adsorbed on the surface. The second large weight-loss step of 18 %, which occurs between 460 and 650 °C, can be ascribed to the combustion of residual carbon. In contrast to the above steps, a weight increase of 7 % occurs in the temperature range of 650 to 960 °C, and is probably related to the oxidation of SiC. These results are consistent with the low Si/C ratio in the mesoporous SiC replicas, implying that carbon residues are burnt in air and a small amount of oxygen is simultaneously introduced.

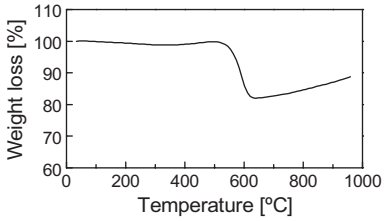

Figure 6. TGA curve of a SiC-KIT6-1400 sample under air.

2.3. Porosity

Mesoporous SiC replicas synthesized by this one-step nanocasting method exhibit very large BET surface areas and narrow pore-size distributions, as shown in Figure 7 and Table 1. It should be noted that the isotherms of mesoporous silicon carbides derived from KIT-6, which had been hydrothermally treated at 130 °C, display two evident capillary condensation steps (Figs. 7g,h). Bimodal pore-size distributions can therefore

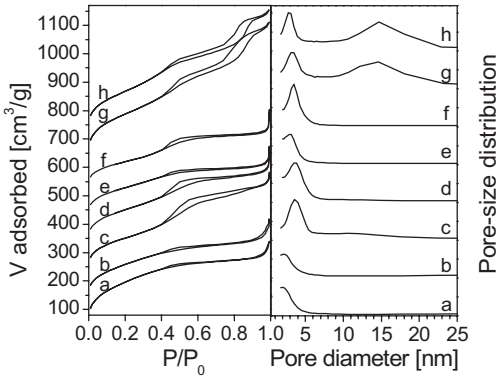

Figure 7. Nitrogen-sorption isotherms and pore-diameter distribution curves of mesoporous SiC ceramics. The letters a–h correspond to those listed in Table 1. Each curve is offset along the *y*-axis by 100 cm^3 g^{-1} relative to the previous curve. *V*: volume; P/P_0: relative pressure.

be plotted at mean values of 3.0 and 15 nm, respectively. This is similar to the case for mesoporous carbon replicas prepared from a silica host that had been treated hydrothermally at 130 °C.[30] The bimodal pore-size distribution may be attributed to the formation of large mesoscale tunnels in the silica wall during the long hydrothermal treatment at high temperature. Comparing the pore-size distribution of KIT-6 that had been hydrothermally treated at 130 °C with a conventionally treated sample that was treated at 100 °C (Figs. 8c,d), the porosity texture is obviously different, the mean pore size increases from

© 2006 WILEY-VCH Verlag GmbH & Co. KGaA, Weinheim

ADVANCED FUNCTIONAL MATERIALS

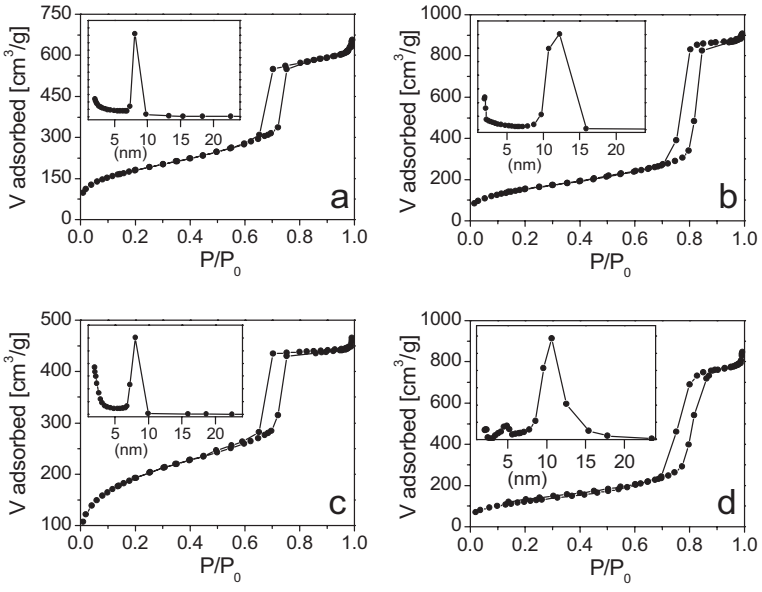

Figure 8. Nitrogen-sorption isotherms and pore-size distributions (insets) of mesoporous silica templates: a) SBA-15 hydrothermally treated at 100 °C; b) SBA-15 hydrothermally treated at 130 °C; c) KIT-6 hydrothermally treated at 100 °C; and d) KIT-6 hydrothermally treated at 130 °C.

8 to 11 nm and a new, small peak appears at around 3–6 nm in the pore-size distribution. This indicates that mesopores of about 5 nm are generated in the silica walls upon increasing the hydrothermal temperature and extending the time of the hydrothermal treatment. The treatment can, furthermore, enhance the mesostructural regularity (Fig. 9b). Silicon carbides whose mother template is KIT-6 that had been hydrothermally treated at 100 °C and have only one narrow pore-size distribution (Figs. 7e,f), show much smaller pore volumes and BET surface areas than those derived from KIT-6 treated at 130 °C, implying a rather lower structural regularity in the former samples. The absence of the secondary mesopores in the silica walls results in weak interconnections of SiC and distinct structural shrinkage after removal of the silica templates, as observed in the small-angle XRD patterns of the products (Fig. 9b).

The effect of the hydrothermal parameters is more remarkable in the case of 2D hexagonal mesoporous materials. In contrast to the highly ordered mesostructure of the SiC replicas copied from SBA-15 that had been hydrothermally treated at 130 °C, only poorly ordered mesoporous SiC products could be achieved (Fig. 9a) when SBA-15 treated at 100 °C was used as the host. Accordingly, the latter possessed significantly smaller pore diameters and volumes than the former, as shown in Table 1. We, again, attribute this fact to the expansion of the micropores to mesopores in the silica walls during the long hydrothermal treatment at high temperature.[29] Unlike the pores in KIT-6 with 3D channels, the replica of which can have self-supported frameworks, the mesopores in the SBA-15 walls are essential to the formation of stable interlinks in the SiC framework. Consequently, the pores inhibit the partial collapse of the mesoscale arrangement caused by a lack of connections. These results suggest that the size and number of mesopores in the silica walls play key roles in the formation of highly ordered mesoporous SiC ceramics in this nanocasting process.

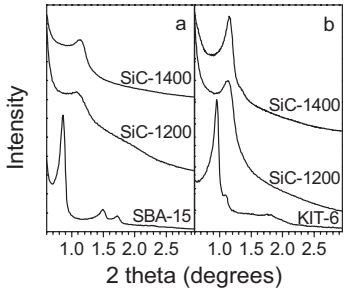

Figure 9. Small-angle XRD patterns of mesoporous silicon carbide replicas (replicated by hydrothermally treating mesoporous silica at 100 °C) and their mother mesoporous silica templates with a) a 2D hexagonal (*p6m*) structure and b) a 3D cubic (*Ia3d*) structure.

Compared with the other synthetic processes, such as chemical vapor deposition (CVD) and carbothermic reduction, our method allows fabrication of silicon carbides with extraordinarily high BET surface areas (up to 720 $m^2 g^{-1}$).[16] In CVD and carbothermic reduction, well-grown large SiC crystals with glazed surfaces possibly develop because of the participation of gaseous reactants, which are generated from gaseous raw materials such as SiH_4, or from intermediate species such as SiO. Both the large crystal size and the glazed surface of SiC dramatically reduce the surface area. In our method, however, concretionary amorphous SiC solids that have no fluidic properties are first produced during the pyrolysis of the polymeric precursors. The crystallization that follows is achieved by the local reassembly of Si–C bonds. Therefore, the glazed surface would not be formed in this instance. Taking into account the yield point of PCS, the nanocasting process is carried out at 300 °C for 5 h, so that the rough surface of the silica hosts could be entirely replicated by the PCS guest composites. In the subsequent heating process carried out for solidification, the shapes of the channels in the mother mesoporous silica are fully copied to the SiC. Hence, rough surfaces of the SiC nanowires can be obtained after removal of the silica matrix, resulting in an unusually high surface area. This can, in turn, confine the growth of SiC nanowires within the mesochannels in the silica templates and prevent the aggregation of the nanoparticles, which can improve the surface area.

2.4. Pyrolysis Procedure

The heating process is essential for synthesis of highly ordered mesoporous SiC ceramics. In order to determine the pyrolysis characteristics of the polymeric precursor, TGAs of PCS under nitrogen atmosphere have been conducted. The main weight loss in the range 300–700 °C can be associated

 © 2006 WILEY-VCH Verlag GmbH & Co. KGaA, Weinheim

with the escape of small molecules such as CH_4 from bond cleavage of PCS. Almost no further weight loss was detected at temperatures above 700 °C. It was also found that the weight loss depends on the heating rate to a substantial extent. Based on the weight ratio of the final product to the PCS precursor, the total ceramic yield after calcination at 900 °C was enhanced from 58 to 74 % by reducing the heating rate from 10 to 2 °C min^{-1}. This can be attributed to the stronger crosslinking interactions among the PCS molecules at a lower heating rate. Combining this fact with the above-mentioned results, the heating procedure has been optimized to improve the crosslinkage and, in turn, the ceramic yield. The loaded PCS/silica samples were thermally isolated at 300 °C for 5 hours. A secondary calcination step was carried out at up to 700 °C at a rate of 0.5 °C min^{-1}. Finally, the samples were heated up to the final temperature at a rate of 2 °C min^{-1} and the temperature was maintained for 2 h. Such a pyrolysis process gave yields of mesoporous SiC ceramics that were higher than 75 % in all our experiments.

2.5. Thermal Stability

High thermal stability under a nitrogen atmosphere is another predominant feature of the ordered mesoporous SiC ceramics. Figure 10 displays the small-angle XRD patterns of the mesoporous SiC replicas (SiC-1400) before and after re-treatment at 1400 °C under nitrogen for 2 h. Mesoporous SiC replicated from KIT-6 exhibits an excellent thermal stability. The specific surface area (590 $m^2 g^{-1}$) and the pore volume (0.71 $cm^3 g^{-1}$) remain nearly unchanged after re-treatment at 1400 °C. To the best of our knowledge, this is the highest BET surface area for non-oxide ceramics at such a high temperature. The thermal stability of the SiC-SBA15-1400 sample was not as high as that of SiC-KIT6-1400, with the specific surface area and the pore volume decreasing from 544 to 280 $m^2 g^{-1}$ and from 0.58 to 0.40 $cm^3 g^{-1}$, respectively, upon re-treatment. This can be ascribed to the 3D network connections in the latter. However, TEM observations (Fig. 11) showed that even the SBA-15-derived, 1400 °C-re-treated mesoporous SiC shows good mesoscale ordering. The pore-size distributions of the SiC replicas re-treated at 1400 °C become broader (3–9 nm) regardless of the structures of the mother templates.

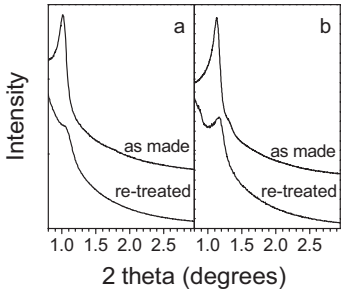

Figure 10. Small-angle XRD patterns of mesoporous silicon carbide ceramics before and after 1400 °C re-treatment for 2 h under N_2: a) SiC-SBA15-1400 and b) SiC-KIT6-1400.

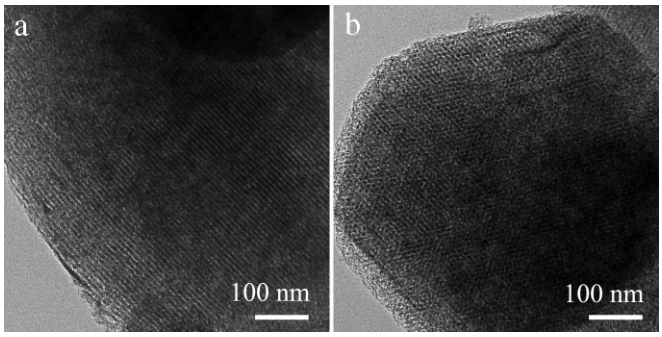

Figure 11. TEM images of calcined mesoporous silicon carbides SiC-SBA15-1400 re-treated at 1400 °C for 2 h under a N_2 atmosphere after removal of the silica matrix by HF etching.

As mentioned above, about 14 % oxygen and some excess carbon have been detected in the final products, from which we deduce that silicon reacted with nitrogen via a carbothermic reduction.[31] XRD and optical microscopy measurements show that villiform silicon nitrides formed on the surface of the SiC powder piles and the crucible when the SiC products were heated at 1400 °C under a N_2 atmosphere. During the heating process, silicon, oxygen, and carbon atoms escaped from the framework as gaseous intermediates in the form of SiO and CO, which then could have reacted carbothermically with nitrogen gas on the surface of the sample, resulting in the villiform silicon nitrides. These Si_3N_4 can fortunately be removed during HF etching, as can be seen from TEM and XRD measurements. Therefore, the decrease of the framework density as a result of atoms escaping does not facilitate a decrease in the specific surface area in the mesoporous SiC, despite the framework shrinkage that can occur at 1400 °C during the heat re-treatment (Fig. 10). As a result, the pore-size distribution becomes broader.

3. Conclusions

Two kinds of highly ordered mesoporous silicon carbides with high specific surface areas (up to 720 $m^2 g^{-1}$), large pore volumes (up to 0.8 $cm^3 g^{-1}$), and narrow pore-size distributions (mean value of ~3.5 nm) have been successfully prepared by a one-step nanocasting method, using PCS as a precursor and mesoporous silica as hard templates. Small-angle XRD patterns and TEM images reveal that 2D hexagonal (*p6m*) and 3D bicontinuous (*Ia3d*) mesostructured SiC ceramics can replicate well the mesoporous channels of the silica hosts, and have extraordinary thermal stability up to 1400 °C under nitrogen atmosphere.

4. Experimental

Triblock poly(ethylene oxide)-*b*-poly(propylene oxide)-*b*-poly(ethylene oxide) copolymer Pluronic P123 (weight-average molecular weight (M_w) = 5800, $EO_{20}PO_{70}EO_{20}$) was obtained from Aldrich Chemical Inc. PCS (M_n = 1500, yield point = 218–247 °C) was bought from Key

© 2006 WILEY-VCH Verlag GmbH & Co. KGaA, Weinheim

ADVANCED FUNCTIONAL MATERIALS

Lab of Ceramic Fiber and Composites, National University of Defense Technology. Other chemicals were purchased from Shanghai Chemical Company. All chemicals were used as received without any further purification.

Synthesis of Mesoporous Silica SBA-15: SBA-15 hard templates were prepared by hydrothermal synthesis according to the established procedures [27]. 25.0 g of triblock copolymer P123 was dissolved in 770 mL of water and stirred overnight. The solution was heated to 38 °C and 110 mL of 37 wt.-% HCl was added. After 1 h, 54.0 g of TEOS (tetraethyl orthosilicate) was poured in while stirring rigorously, and the mixture was kept at the same temperature for 24 h. The solution was then transferred into a stainless-steel autoclave and heated to 100 °C or 130 °C for 3 days. The white solids were recovered by filtration, washed with deionized water, and dried. Thereafter, the products were calcined at 550 °C for 5 h at a heating rate of 1.5 °C min^{-1} in air.

Synthesis of Cubic Mesoporous Silica KIT-6 [28]: To 23.5 g of triblock copolymer P123 and 850 mL of water, which was dissolved at 35 °C overnight, 38.0 mL of 37 wt.-% HCl and 23.5 g *n*-butanol were added. The mixture was kept stirring for 2 h. 48.0 g of TEOS was added under vigorous stirring. The rest of the procedure was the same as for SBA-15.

Nanocasting: First, 6.0 g of PCS was dissolved in 60 g xylene. 5.0 g of mesoporous silica host (SBA-15 or KIT-6) was then mixed in well under stirring. After the organic solvent xylene was evaporated, the products were dried in an oven at 100 °C overnight. The acquired PCS/silica composite was first heated at a rate of 2 °C min^{-1} to 300 °C under a N_2 flow, and then the temperature was maintained for 5 h. A further heating process to 700 °C was carried out at a rate of 0.5 °C min^{-1} for the crosslinking and pyrolyzing of PCS. Lastly, the temperature was raised to the final value for crystallization at a heating rate of 2 °C min^{-1} and the temperature was kept for 2 h. The resulting SiC–silica composite was washed with 10 wt.-% aqueous hydrofluoric acid several times to remove the silica template.

Characterization: Small-angle powder XRD patterns were recorded by a Bruker D4 powder X-ray diffractometer using Cu Kα radiation. Nitrogen adsorption–desorption isotherms were measured on a Micromeritics Tristars 3000 analyzer at 77 K. Before the measurements, the samples were outgassed at 200 °C in vacuum for 6 h. The BET method was utilized to calculate the specific surface area. The pore-size distributions were derived from the adsorption branches of the isotherms using the Barrett–Joyner–Halanda (BJH) method. The total pore volumes, V_p, were estimated from the amount adsorbed at a relative pressure of $P/P_0 = 0.95$. TEM measurements were conducted on a JEOL 2011 microscope operated at 200 kV. All samples were first dispersed in ethanol, and then collected using copper grids covered with carbon films for analysis. The oxygen content of the products was determined using a TC600 Nitrogen/Oxygen Determinator (LECO). The silicon and carbon contents were determined by chemical analysis. TG analyses were carried out on a Mettler Toledo TGA/SDTA851 apparatus under either nitrogen or air flow at a rate of 40 or 80 mL min^{-1}, respectively. FTIR spectra of mesoporous SiC products in a KBr tablet were recorded on a FTIR360 (Nicolet) spectrometer.

Received: June 6, 2005
Final version: October 18, 2005
Published online: January 3, 2006

[1] H. Klemm, C. Taut, G. Wotting, *J. Eur. Ceram. Soc.* **2003**, *23*, 619.
[2] K. Watari, *J. Ceram. Soc. Jpn.* **2001**, *109*, S7.
[3] H. Klemm, M. Herrmann, C. Schubert, *J. Eng. Gas Turbines Power* **2000**, *122*, 13.
[4] K. G. Nickel, *Ceram. Int.* **1997**, *23*, 127.
[5] C. H. Bates, M. R. Foley, G. A. Rossi, G. J. Sundberg, F. J. Wu, *Am. Ceram. Soc. Bull.* **1990**, *69*, 350.
[6] M. B. Kizling, P. Stenius, S. Andersson, A. Frestad, *Appl. Catal. B* **1992**, *1*, 149.
[7] L. Pesant, J. Matta, F. Garin, M. J. Ledoux, P. Bernhardt, C. Pham, C. Pham-Huu, *Appl. Catal. A* **2004**, *266*, 21.
[8] N. Keller, C. Pham-Huu, C. Estornes, M. J. Ledoux, *Appl. Catal. A* **2002**, *234*, 191.
[9] M. J. Ledoux, C. Crouzet, C. Pham-Huu, V. Turines, K. Kourtakis, P. L. Mills, J. J. Lerou, *J. Catal.* **2001**, *203*, 495.
[10] N. Keller, C. Pham-Huu, M. J. Ledoux, *Appl. Catal. A* **2001**, *217*, 205.
[11] M. J. Ledoux, C. Pham-Huu, N. Keller, J. B. Nougayrede, S. Savin-Poncet, J. Bousquet, *Catal. Today* **2000**, *61*, 157.
[12] N. Keller, C. Pham-Huu, C. Crouzet, M. J. Ledoux, S. Savin-Poncet, J. B. Nougayrede, J. Bousquet, *Catal. Today* **1999**, *53*, 535.
[13] C. Pham-Huu, C. Bouchy, T. Dintzer, G. Ehret, C. Estournes, M. J. Ledoux, *Appl. Catal. A* **1999**, *180*, 385.
[14] C. Methivier, B. Beguin, M. Brun, J. Massardier, J. C. Bertolini, *J. Catal.* **1998**, *173*, 374.
[15] F. Cheng, S. M. Kelly, F. Lefebvre, S. Clark, R. Supplit, J. S. Bradley, *J. Mater. Chem.* **2005**, *15*, 772.
[16] K. H. Park, I. K. Sung, D. P. Kim, *J. Mater. Chem.* **2004**, *14*, 3436.
[17] P. Krawiec, C. Weidenthaler, S. Kaskel, *Chem. Mater.* **2004**, *16*, 2869.
[18] M. Kamperman, C. B. W. Garcia, P. Du, H. S. Ow, U. Wiesner, *J. Am. Chem. Soc.* **2004**, *126*, 14 708.
[19] F. Cheng, S. Clark, S. M. Kelly, J. S. Bradley, F. Lefebvre, *J. Am. Ceram. Soc.* **2004**, *87*, 1413.
[20] G. Q. Jin, X. Y. Guo, *Microporous Mesoporous Mater.* **2003**, *60*, 207.
[21] P. Dibandjo, L. Bois, F. Chassagneux, D. Cornu, J. M. Letoffe, B. Toury, F. Babonneau, P. Miele, *Adv. Mater.* **2005**, *17*, 571.
[22] Z. C. Liu, W. H. Shen, W. B. Bu, H. R. Chen, Z. L. Hua, L. X. Zhang, L. Lei, J. L. Shi, S. H. Tan, *Microporous Mesoporous Mater.* **2005**, *82*, 137.
[23] F. Cao, D. P. Kim, X. D. Li, *J. Mater. Chem.* **2002**, *12*, 1213.
[24] R. J. Ciora, B. Fayyaz, P. K. T. Liu, V. Suwanmethanond, R. Mallada, M. Sahimi, T. T. Tsotsis, *Chem. Eng. Sci.* **2004**, *59*, 4957.
[25] H. Wang, X. D. Li, T. S. Kim, D. P. Kim, *Appl. Phys. Lett.* **2005**, *86*, 173 104.
[26] H. Wang, J. S. Yu, X. D. Li, D. P. Kim, *Chem. Commun.* **2004**, 2352.
[27] D. Y. Zhao, J. L. Feng, Q. S. Huo, N. Melosh, G. H. Fredrickson, B. F. Chmelka, G. D. Stucky, *Science* **1998**, *279*, 548.
[28] F. Kleitz, S. H. Choi, R. Ryoo, *Chem. Commun.* **2003**, 2136.
[29] J. Fan, C. Z. Yu, L. M. Wang, B. Tu, D. Y. Zhao, Y. Sakamoto, O. Terasaki, *J. Am. Chem. Soc.* **2001**, *123*, 12 113.
[30] C. Z. Yu, J. Fan, B. Z. Tian, D. Y. Zhao, G. D. Stucky, *Adv. Mater.* **2002**, *14*, 1742.
[31] S. Shimada, T. Kataoka, *J. Am. Ceram. Soc.* **2001**, *84*, 2442.

© 2006 WILEY-VCH Verlag GmbH & Co. KGaA, Weinheim